Ab Initio Study of the Mechanism and Thermochemistry of the Atmospheric Reaction $NO + O_3 \rightarrow NO_2 + O_2$

Julio Peiró-García and Ignacio Nebot-Gil*

Instituto de Ciencia Molecular, Departamento de Química Física, Facultad de Química, Universidad de Valencia, c/ Dr. Moliner, 50, E-46100, Burjasot (Valencia), Spain

Received: February 18, 2002; In Final Form: June 17, 2002

The atmospheric reaction between NO and ozone has been investigated using ab initio methods. The structures of all reactants, products, intermediates, and transition states of reaction 1 have been optimized and characterized at the UMP2(full) level of theory. The 6-31G(d), 6-311G(d), and 6-311G(df) basis sets have also been used to calibrate the effect of the basis set functions on the optimized structures and energies of all stationary points. Finally, we have reoptimized at the UMP4(SDQ, full)/6-31G(d) and 6-311G(d) levels. The energetics of the reaction has been studied more accurately within the G2 and G2(MP2) schemes. Also, QCISD(T)/6-311G(d) single-point calculations have been performed by using UMP2(full)/6-31G(d), 6-311G(d), and 6-311G(df) geometries. The mechanism study of the $NO + O_3 \rightarrow NO_2 + O_2$ reaction has shown that the transition between reactants and products is not direct, but it proceeds along two transition states (**TS1** and **TS2**) separated by the intermediate (**A**). There is also the possibility of two different conformational (cis/trans) channels on the PES. In addition to the title reaction (the only one found under atmospheric conditions), we have also extended our QCISD(T)/6-311G(d)//UMP2(full)/6-31G(d) study to the reactions that might occur under high temperature or pressure conditions, such as $NO + O_3 \rightarrow NO_2 + O_2(^1\Delta_g)$, $NO + O_3 \rightarrow ONOO + O(^3P)$, $ONOO \rightarrow NO + O_2$, $ONOO \rightarrow NO_2 + O(^3P)$, and $ONOO \rightarrow NO_3$.

1. Introduction

General knowledge of atmospheric chemistry[1] has become very important in recent years because of its fundamental implication on the environment and its effects on a variety of aspects related to life, such as health, biodiversity, and economics.

Nitrogen oxides (NO_x) play an important role in tropospheric chemistry. However, despite the extensive experimental research made on reactions of NO_x, theoretical studies are very scarce in the literature.[2−4]

The atmospheric reaction

$$NO + O_3 \rightarrow NO_2 + O_2(^3\Sigma_g^-) \quad (1)$$

is of fundamental importance because the majority of the NO_x emitted into the atmosphere (at least 95%, as generally accepted) is in the form of the primary pollutant NO because ozone is the most abundant photochemical oxidant and because the reaction between them is very fast.

However, the most important implication that reaction 1 has in the tropospherical chemistry of NO_x is due to the fact that NO_2 photolysis is an important source of ozone pollution in the troposphere[5−7] through the displacement of the Leighton equilibrium.[6−8]

Although $NO_2 + O_2(^3\Sigma_g^-)$ are the only products experimentally found for the reaction between NO and O_3, we have included in our study different reaction channels that might occur under higher temperature conditions, such as

$$NO + O_3 \rightarrow NO_2 + O_2(^1\Delta_g) \quad (2)$$

$$NO + O_3 \rightarrow ONOO + O(^3P) \quad (3)$$

$$ONOO \rightarrow NO + O_2 \quad (4)$$

$$ONOO \rightarrow NO_2 + O(^3P) \quad (5)$$

$$ONOO \rightarrow NO_3 \quad (6)$$

Reaction 1 is also relevant to the stratosphere because the NO_x emitted from supersonic transports (SST) can easily react, destroying the ozone layer in a catalytic cycle[9] similar to that proposed for Cl atoms:

$$NO + O_3 \rightarrow NO_2 + O_2$$
$$\underline{NO_2 + O \rightarrow NO + O_2}$$
$$O_3 + O \rightarrow 2O_2$$

Because of its implications in atmospheric chemistry and the visible chemiluminescence it shows,[10] reaction 1 has been extensively studied. It was first assumed that reaction 1 took place along two different PESs with different rate coefficients and activation energies:

$$NO + O_3 \rightarrow NO_2(^2A_1) + O_2$$

$$NO + O_3 \rightarrow NO_2^*(^2B_2) + O_2$$

$$NO_2^* \rightarrow NO_2 + h\nu$$

However, Adler-Golden[11] has shown that the experimental data can be explained in terms of a single PES. This is mainly

* Corresponding author. E-mail: ignacio.nebot@uv.es.

10.1021/jp020422q CCC: $22.00
Published on Web 10/04/2002

due to the great mixing between the $^2B_2$ excited electronic state of NO_2 and the high vibrational levels of the ground $^2A_1$ state. In any case, because we cannot introduce the appropriate coupling between the two states, in this work we will restrict our study of the mechanism to the fundamental PES of NO_2.

Because of its important implications to atmospheric chemistry, considerable research effort[12−20] has been devoted to measuring the rate of reaction 1. All the measured rate constants lie within the range $1.41 \times 10^{-14}-2.77 \times 10^{-14}$ cm^3 molecule^{-1} s^{-1}, and all activation energies lie within the range 1.44−3.18 kcal/mol. The IUPAC-recommended Arrhenius expression for the rate coefficient is[21] $k = 1.8 \times 10^{-12} \exp(-1370/T)$ cm^3 molecule^{-1} s^{-1}. Then, at 298.15 K, $k^{298.15k} = 1.8 \times 10^{-14}$ cm^3 molecule^{-1} s^{-1}, and $E_a^{298.15k} = 2.72$ kcal/mol. This expression is based on a least-squares analysis of the data over the range 195−304 K.[16−20] The temperature range is limited because Clyne et al.,[12] Clough and Thrush,[13] Birks et al.,[16] Michael et al.,[19] and Borders and Birks[20] found a nonlinear Arrhenius behavior that can be represented as $k = 8.9 \times 10^{-19} T^{2.2} \exp(-765/T)$ cm^3 molecule^{-1} s^{-1}. [22]

In this paper, theoretical results derived from a high-level ab initio study of the mechanism of reactions 1−6 are presented. Theoretical and computational details are described in section 2. The results are discussed in section 3 as follows: In subsection 3.1, we focus on reaction 1, in subsection 3.2, we describe reaction 2, and in subsection 3.3, we discuss reactions 3−6. The main conclusions that arise from the current research are finally summarized in section 4.

2. Computational Details

Geometries of all stationary points involved in the mechanism of reactions 1−6 have been previously optimized with the semiempirical AM1[23] method because of the complexity of the reaction mechanism and because it has been shown that this method efficiently works with radicals.[24] All AM1 calculations have been performed with the MOPAC 93[25] program.

The geometries obtained have then been reoptimized at the UHF,[26] B3LYP,[27] UMP2,[28] and UMP4(SDQ,full) levels of theory with the 6-311G(d)[29] basis set. Unfortunately, despite the great recent advances made in density functional theory (DFT), which is particularly relevant when dealing with radicals, the B3LYP method was not able to reoptimize most of the saddle points previously found at the UHF or UMP2 levels. Becke's three-parameter hybrid[30] method B3PW91[31] and the local spin-density approximation (LSDA) [32] were also tested. However, the results obtained with these methods were similar to those obtained with B3LYP; therefore, we finally decide to obviate DFT methods in further research.

To check the convergence of the predicted structures and relative energies calculated for reaction 1 at the level of computation, all stationary points have also been optimized at the UMP2(full)/6-31G(d), 6-311G(df), and UMP4(SDQ,full)/6-31G(d) levels of theory.

The Berny[33] algorithm has been employed for the UHF, MP2, and MP4 geometry optimizations. The computed stationary points have been characterized as minima or transition states by diagonalizing the Hessian matrix and analyzing the vibrational normal modes. In this way, the stationary points can be classified as minima if no imaginary frequencies are shown or as transition states if only one imaginary frequency is obtained. The particular nature of the transition states has been determined by analyzing the motion described by the eigenvector associated with the imaginary frequency. Furthermore, the intrinsic reaction coordinate (IRC)[34] method has been used to describe minimum-energy paths from transition-state structures to the corresponding minima at the UMP2(full)/6-311G(d) level of theory. The eigenfollowing and TS[35] methods have been employed for locating the minima and transition-state structures.

Zero-point energies (ZPE) have also been calculated at these levels of theory. To predict more reliable values, the raw calculated ZPE values were scaled by 0.9676 when the 6-31G(d) basis set was used and by 0.9748 with the 6-311G(d) basis set to account for their average overestimation.[36] To obtain the energies at 298.15 K, the thermal energy of each species has been added to its total energy.

The relative energies calculated for all stationary points of reactions 1−6 have been refined using the G2(MP2)[37] and G2[38] procedures developed by Pople et al.

The best results, however, have been obtained by performing direct QCISD(T)[39] or CCSD(T)[40] single-point energy calculations at the optimized UMP2 structures.

All calculations have been performed with the Gaussian 94[41] set of programs on an IBM RS6000/SP and an SGI Origin 2000 of the theoretical chemistry group of the University of Valencia (Spain).

3. Results and Discussion

Because of the complexity of reactions 1−6, a previous exploration of the PES has been performed with the semiempirical AM1 method in order to characterize all stationary points easily according to their significance in the reaction mechanism. Then, the geometry of all reactants, products, intermediates, and saddle points involved in the reaction between NO and O_3 have been reoptimized at the UHF, UMP2, and UMP4 levels of theory. Also, because of the ability of DFT-based methods to overcome spin-contamination problems, we have tried these methods without successful results.

3.1. Reaction 1: NO + O_3 → NO_2 + $O_2(^3\Sigma_g^-)$. In Figure 1, we depict our proposal of the mechanism of reaction 1. The main geometrical parameters predicted at the UMP2(full)/6-31G(d) level of theory are given along with the geometries of all stationary points and the notation system employed also in Figure 1.

Tables 1 and 1S (Supporting Information) show the optimized geometries of reactants, transition states, intermediates, and products of reaction 1. The calculations have been carried out at the UHF, UMP2(full), and UMP4(SDQ,full) levels of theory using the valence triple-ζ 6-311G(d) basis set with all three methods: the 6-31G(d) at the UMP2 and UMP4 levels of theory and the 6-311G(df) at the UMP2(full) level to analyze the effect of the inclusion of polarization functions on both the structure of the stationary points and the calculated barrier heights of reaction 1.

Finally, Table 2S (Supporting Information) collects the normal-mode frequencies of all the stationary points of reaction 1 calculated at the same levels of theory. Experimental values are also shown in the same table.

3.1.1. Reactants and Products. The UMP2(full) and the UMP4(SDQ,full) optimized structures are in reasonably good agreement with experimental results.[42,43] Therefore, the UMP2-(full) and UMP4(SDQ,full) methods should be good enough to study the mechanism of reaction 1. The best results were obtained with the largest 6-311G(df) basis set, which predicts very accurate values for all the geometrical parameters.

The values given in Table 2S for the vibrational frequencies show, however, three anomalous predictions for NO and the b_2 normal mode of O_3 and NO_2. These discrepancies can be attributed in the case of NO and NO_2 to spin contamination of

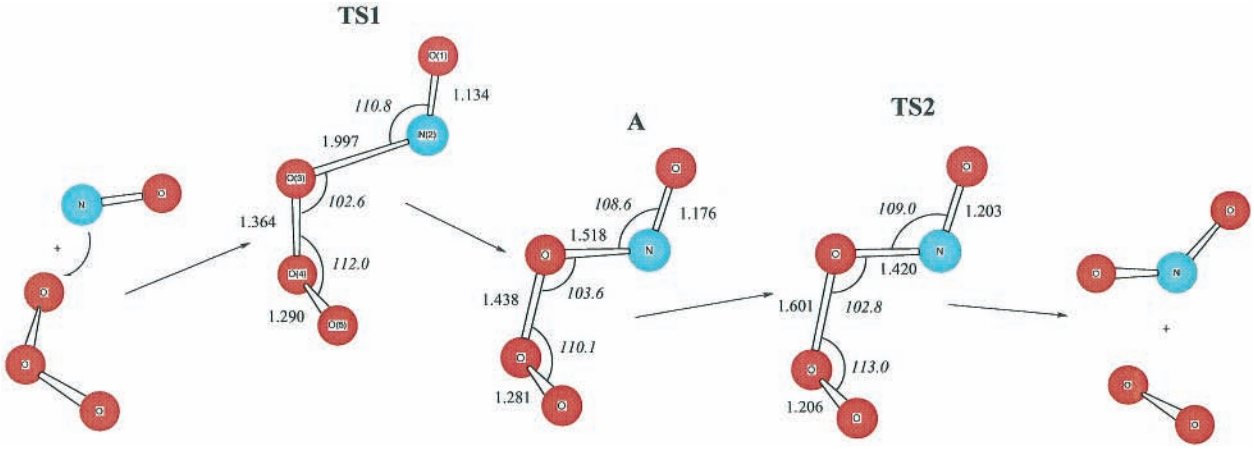

Figure 1. Optimized UMP2(full)/6-31G(d) geometries of the stationary points along the NO + O_3 → NO_2 + $O_2(^3\Sigma_g^-)$ reaction pathway. Angles and dihedrals are given in degrees, and bond distances are given in angstroms.

TABLE 1: Geometrical Parameters[a] of the Reactants and Products of the NO + O_3 → NO_2 + O_2 Reaction

parameter	UHF 6-311G(d)	UMP2[b] 6-31G(d)	UMP2 6-311G(d)	UMP2 6-311G(df)	UMP4 6-31G(d)	UMP4 6-311G(d)	exp[c]
NO							
r(N−O)	1.117	1.143	1.134	1.133	1.146	1.137	1.151
O_3							
r(O−O)	1.194	1.300	1.281	1.273	1.269	1.250	1.278
∠(O−O−O)	119.2	116.3	116.9	117.1	117.5	117.8	116.8
NO_2							
r(N−O)	1.156	1.216	1.202	1.197	1.208	1.194	1.193
∠(O−N−O)	136.3	133.8	134.0	134.3	134.2	134.5	134.1
O_2							
r(O−O)	1.157	1.246	1.223	1.217	1.224	1.204	1.207

[a] Bond lengths are given in angstroms; angles and dihedrals are given in degrees. [b] UMP2 and UMP4(SDQ) optimizations have been performed using all electrons in the correlation. [c] Experimental data taken from refs 47 and 48.

the UHF wave function[44] and in the case of O_3, to the multiconfigurational nature of the wave function, as is well-known.[45]

3.1.2. Reaction Mechanism. As seen in Figure 1, the NO radical approach to the O_3 molecule is determined by the π orbitals of the terminal oxygen atom of ozone, according to the previous theoretical work of Dupuis et al.[46] for the H + O_3 reaction.

The first step of the reaction mechanism is **TS1**, which as expected for exothermic reactions,[47] shows very small perturbations of geometrical parameters compared to those of reactants.

The characterized structure of **TS1** is quite similar to the nonplanar structure reported for the H + O_3[46] and Cl + O_3[48] reactions. The UMP2/6-31G(d) value for the imaginary frequency corresponding to the reaction coordinate is 352.9i cm^{-1}. **TS1** has not been characterized at the UMP4/6-311G(d) level of calculation because of the great computational cost involving this calculation.

To asses the reliability of UMP2 and UMP4 methodologies, **TS1** has also been optimized at the QCISD/6-31G(d) level, confirming the results previously obtained.

The subsequent IRC calculation confirms that **TS1** connects the reactants with the intermediate structure **A**. This is in agreement with the reaction mechanism proposed for the Cl + O_3[48] reaction that proceeds along several steps at the MP2 level.

TS1 has C_1 symmetry. However, except for the O_5 atom, the atoms of **TS1** are almost planar, as can be inferred from the dihedral ∠(O_4−O_3−N_2−O_1) value of −178.3° at the MP2/6-31G(d) level of theory.

The evolution of **TS1** is thus toward an ONOOO intermediate. This point (**A**) has been characterized as a minimum and is the intermediate of reactions 1−3:

$$NO + O_3 \rightarrow [ONOOO] \rightarrow NO_2 + O_2(^3\Sigma_g^-) \quad (1)$$

$$NO + O_3 \rightarrow [ONOOO] \rightarrow NO_2 + O_2(^1\Delta_g) \quad (2)$$

$$NO + O_3 \rightarrow [ONOOO] \rightarrow ONOO + O(^3P) \quad (3)$$

The symmetry of **A** is also C_1, although except for the O_5 atom, the rest of the molecule lies in a plane, as shown by the value of the dihedral angle ∠(O_4−O_3−N_2−O_1) of 180.0° at the UMP2(full)/6-31G(d) theoretical level.

From the intermediate **A**, the products are finally reached through the transition state **TS2**. This saddle point shows an imaginary frequency of 1245.7i cm^{-1} at the UMP2/6-31G(d) level of theory. The spin-density analysis of **TS2** shows two unpaired electrons on the forming $O_2(^3\Sigma_g^-)$ molecule.

The increase of the number of polarization functions from the 6-311G(d) to the 6-311G(df) basis set at the UMP2 level of theory produces structures for **TS1** that are more similar to those of reactants. The changes in the structure of **A** and **TS2** are, however, less sensitive to the number of polarization functions introduced into the basis set.

The change of the double-ζ basis set by a triple-ζ basis set at either the UMP2 or UMP4 level also gives structures for **TS1** that are more similar to those of reactants.

The study of reaction 1 has also shown that there are two different conformational (cis/trans) channels on the PES. As

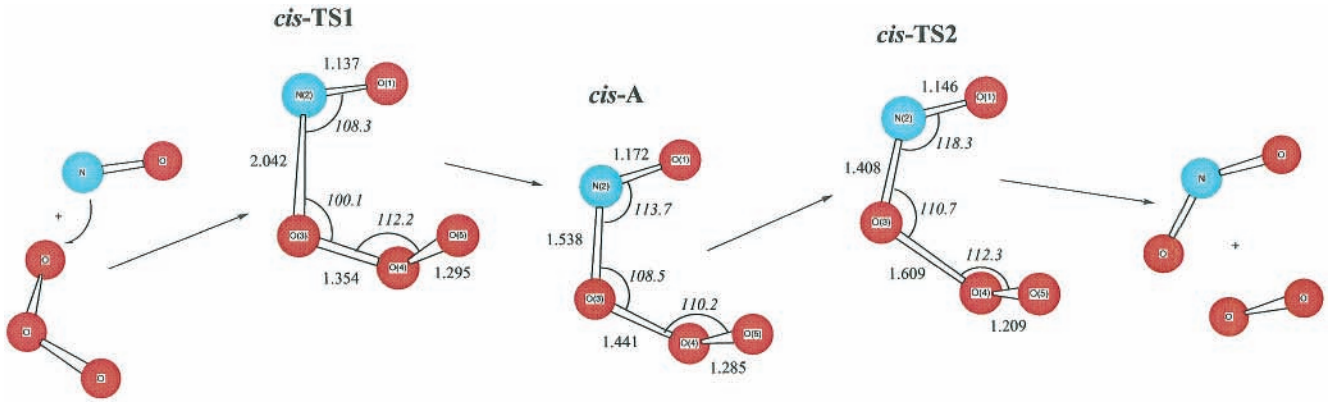

Figure 2. Optimized *cis*-UMP2(full)/6-31G(d) geometries of the stationary points along the NO + O_3 → NO_2 + $O_2(^3\Sigma_g^-)$ reaction pathway. Angles and dihedrals are given in degrees, and bond distances are given in angstroms.

TABLE 2: Vibrational Frequencies (cm^{-1}) of the Stationary Points of the NO + O_3 → NO_2 + O_2 Reaction along the cis and trans Reaction Channels at the MP2/6-31G(d) Level of Theory

method	frequencies (cm^{-1})
cis-**TS1**	333.7i, 118.0, 154.8, 228.5, 449.1, 667.0, 1060.3, 1138.6, 3643.1
trans-**TS1**	352.9i, 73.6, 125.4, 227.9, 345.2, 667.7, 1101.3, 1171.4, 3774.8
cis-**A**	125.7, 279.7, 314.9, 600.2, 649.3, 842.9, 1174.5, 1748.2, 1827.0
trans-**A**	96.9, 189.1, 327.2, 535.4, 669.2, 922.9, 1185.1, 1730.0, 1935.9
cis-**TS2**	1273.3i, 102.7, 250.6, 309.2, 500.1, 595.5, 859.6, 1568.8, 3972.1
trans-**TS2**	1245.7i, 93.7, 168.6, 274.4, 544.2, 631.4, 858.9, 1604.7, 1746.4

can be seen in Figure 1, except for the O_5 atom, all the atoms of any of the stationary points **TS1**, **A**, or **TS2** lie in a plane. Therefore, O_1-O_2 and O_3-O_4 bonds can adopt either cis- or trans-like conformations.

The cis channel on the PES has been studied only at the UMP2(full)/6-31G(d) level of theory. The mechanism and optimized geometries of this new pathway have been depicted in Figure 2. The vibrational normal modes of the optimized stationary points of this channel, cis-**TS1**, cis-**A**, and cis-**TS2**, are shown in Table 2 along with those for the trans channel.

3.1.3. Reaction Enthalpy and Barrier Heights. The QCISD-(T)/6-311G(2d)//UMP2(full)/6-31G(d) energy diagram of reaction 1 is depicted in Figure 3 for both the cis and trans PES channels. The reaction enthalpy and relative energies of **TS1**, **A**, and **TS2** with respect to the reactants NO + O_3 calculated at several levels of theory are shown in Table 3.

The UMP2 barrier height for **TS1**, which is the rate-determining step of reaction 1, calculated with several basis sets is much larger than the experimental values. Projecting out spin contamination reduces calculated barrier heights. However, PUMP2 barriers are still excessively large. The problem is located in the ozone multiconfigurational nature of the wave function.

At the UMP4 level, the rate-determining barrier height also corresponds to **TS1**. However, at this level of theory, the **TS1** and **TS2** barrier heights are also overestimated. Moreover, with the inclusion of triples, the UMP4 barrier height value for **TS1** drops to 28.7 kcal/mol, as can be seen in Table 3.

Because of this important limitation of perturbational Möller−Plesset methods, G2(MP2) and G2 calculations have been carried out on every stationary point of the PES. These methodologies give, respectively, maximum barrier heights of 6.94 and 6.22 kcal/mol for **TS1**, which are closer to the experimental recommended value.

The G2 technique reproduces results of a single-point QCISD-(T)/6-311+G(3df,2p) calculation at a frozen UMP2(full)/6-31G-

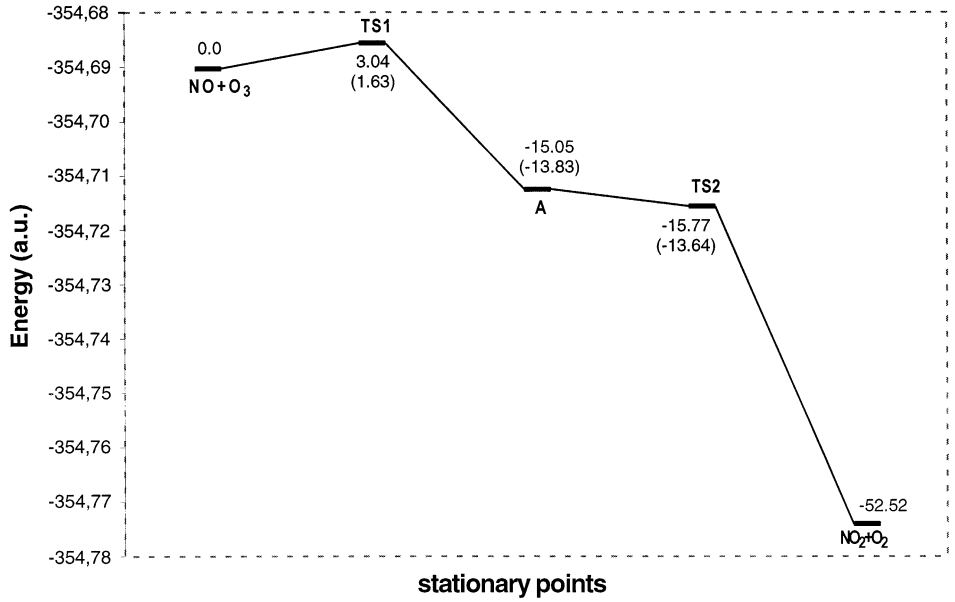

Figure 3. Potential QCISD(T)/6-311G(2d)//UMP2(full)/6-31G(d) energy profile for the reaction between NO and O_3. Relative energies with respect to the reactants NO + O_3 are given in kcal/mol. Values in parentheses refer to the cis potential energy surface. ZPE and thermal corrections are included.

TABLE 3: Reaction Enthalpy ($\Delta H^{o}_{298.15}$), Barrier Heights for Transition States TS1 and TS2, and Stabilization Energy of the Intermediate of the Reaction between O_3 and NO[a]

method	$\Delta H^{\circ}_{298.15}$	$\Delta E_{\mathbf{TS1}}$	ΔE_a	$\Delta E_{\mathbf{TS2}}$
UHF/6-311G(d)[b]	−88.46	−22.96	−28.50	−27.25
MP2(full)/6-31G(d)	−52.48	39.36	1.93	17.84
cis-MP2(full)/6-31G(d)		37.51	−0.40	21.82
PMP2(full)/6-31G(d)	−58.07	23.94	2.09	0.90
MP2(full)/6-311G(d)	−54.61	28.97	4.68	20.84
MP2(full)/6-311G(df)	−52.85	39.03	1.91	19.71
MP4(SDQ,full)/6-31G(d)	−60.56	10.02	−15.96	−6.74
MP4(SDQ,full)/6-311G(d)[c]	−59.98	10.81	−13.32	−2.11
MP4(SDTQ)/6-311G(d)//MP2/6-31G(d)[c]	−52.30	28.71	−2.48	−1.07
G2(MP2)	−43.49	6.94	−11.90	−13.04
G2	−44.31	6.22	−11.79	−23.50
CCSD(T)/6-311G(d)//MP2/6-31G(d)	−54.13	3.83	−11.66	−13.55
cis-CCSD(T)/6-311G(d)//MP2/6-31G(d)		3.23	−11.98	−14.51
QCISD(T)/6-311G(d)//MP2/6-31G(d)	−54.13	3.79	−12.06	−14.53
cis-QCISD(T)/6-311G(d)//MP2/6-31G(d)		3.02	−12.66	−12.46
QCISD(T)/6-311G(d)//MP2/6-311G(d)	−54.23	3.90	−11.37	−12.84
QCISD(T)/6-311G(d)//MP2/6-311G(df)	−52.66	4.94	−11.24	−12.05
QCISD(T)/6-311G(d)//MP4/6-31G(d)	−52.93	4.41	−10.37	−13.32
QCISD(T)/6-311G(d)//MP4/6-311G(d)	−52.62	2.75	−11.60	−12.25
QCISD(T)/6-311G(2d)//MP2/6-31G(d)	−52.52	3.04	−13.83	−15.77
cis-QCISD(T)/6-311G(2d)//MP2/6-31G(d)		1.63	−15.05	−13.64
QCISD(T)/6-311G(3d)//MP2/6-311G(df)	−51.74	3.11	−14.39	−14.80

[a] These energy values are relative to reactants NO + O_3 and are given in kcal/mol. [b] UHF/6-311G(d) relative energies include the ZPE correction but not the thermal correction. [c] MP4(SDQ,full)/6-311G(d) and MP4(SDTQ)/6-311G(d)//MP2(full)/6-31G(d) energies do not include ZPE corrections because of the great computational cost involved in a frequency calculation.

(d) geometry, assuming the additivity of several corrections introduced. However, the G2 scheme is based on UMP4(SDTQ)/6-311G(d) energies, and the corrections are added through MP2 and MP4 calculations when both methods have not described adequately the energetics of reaction 1. Hence, with the aim of predicting more reliable energies, we have carried out CCSD(T)/6-311G(d), QCISD(T)/6-311G(d), 6-311G(2d), and 6-311G(3d) single-point energy calculations. These calculations have been computed by using the frozen geometry of the optimized MP2 and MP4 stationary points.

Single-point QCISD(T)/6-311G(d) energy calculations have been carried out at each MP2 and MP4 geometry, showing that the inclusion of polarization functions in the basis set employed to optimize the geometry of **TS1** at the MP2 level of theory increases the calculated barrier height from 3.9 to 4.9 kcal/mol because the optimized **TS1** structures are situated earlier in the PES, as can be seen in Table 3.

The QCISD(T) and CCSD(T) calculations shows that the cis channel is slightly favored from a kinetic point of view with respect to the trans channel, despite steric repulsion, as can be seen in Table 3.

Lower transition barriers are obtained when using the same UMP2(full)/6-31G(d) geometries but performing QCISD(T) single-point energy calculations with the larger basis set 6-311G(2d) for both the cis and trans channels, as can be seen in Table 3.

Therefore, we can conclude that, at a fixed geometry, if we use an increasing number of polarization functions in the basis set employed for the single-point QCISD(T) or CCSD(T) calculation then the obtained rate-determining barrier height decreases. We have then two opposite effects. The improvement of the geometry quality, which is achieved by increasing the number of polarization functions on the basis set employed during the MP2 optimization, increases the calculated barrier heights at the QCISD(T) level. On the other hand, the use of larger basis sets in the single-point QCISD(T) calculation at a fixed geometry reduces the same barrier. However, all calculated values for the rate-determining transition barrier of reaction 1 lie in the range of the experimentally determined values, between 1.44 and 3.18 kcal/mol.

TABLE 4: Open-Shell T_1 Diagnostic Values for All Stationary Points of the NO + O_3 → NO_2 + O_2 Reaction

species	CCSD(T)/6-311G(d)[a]	CCSD(T)/6-31I1G(d)[b]
NO	0.0261	0.0204
O_3	0.0349	0.0274
TS1	0.0501	0.0525
A	0.0336	0.0301
TS2	0.0511	0.0464
NO_2	0.0275	0.0241
O_2	0.0152	0.0148

[a] UMP2/6-31G(d) optimized geometries. [b] UMP2/6-311G(df) optimized geometries.

The values calculated for the reaction enthalpy of reaction 1 are −52.5, −54.6, and −52.9 kcal/mol, depending on the basis set employed at the MP2 level of theory. These theoretical values differ slightly from the experimentally measured value of −47.6 kcal/mol. However, we can consider that our values are accurate enough if we take into account the fact that the experimentally recommended enthalpy is an average of the value corresponding to the $NO_2(^2A_1)$ ground electronic state and the value corresponding to the $NO_2(^2B_2)$ excited state.

MP4 methodology including triples gives nearly the same results as MP2. G2 and G2(MP2) give values of −43.4 and −44.3 kcal/mol, respectively, above the recommended experimental value. Finally, QCISD(T) and CCSD(T) give results similar to those predicted at the MP2 or MP4(SDTQ) level.

As can be seen in Table 3, at the QCISD(T)/6-311G(d) level, the larger the basis set used along the MP2 or MP4 optimization step, the higher the calculated reaction enthalpy is. The same happens, as well, when the fixed MP2/6-31G(d) geometry is

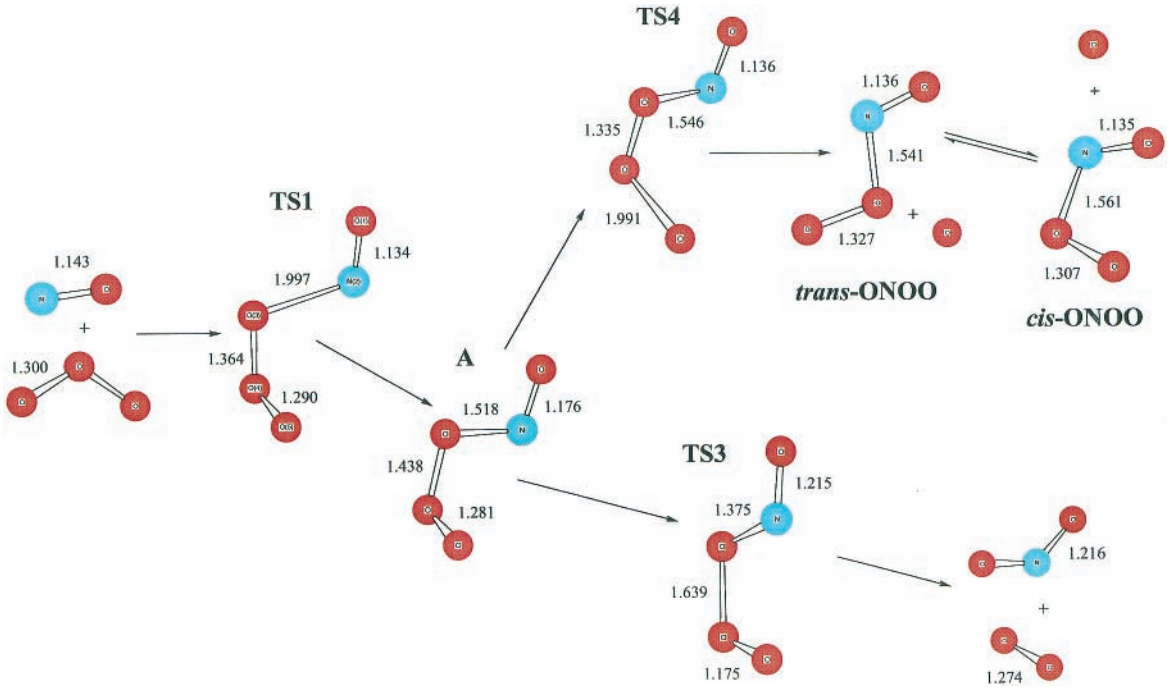

Figure 4. Reaction mechanism for the NO + O_3 → NO_2 + $O_2(^1\Delta_g)$ and NO + O_3 → ONNO + $O(^3P)$ reactions. Evolution of the NO + O_3 system during a hypothetical process that takes place under high-temperature conditions. Bond distances are given in angstroms.

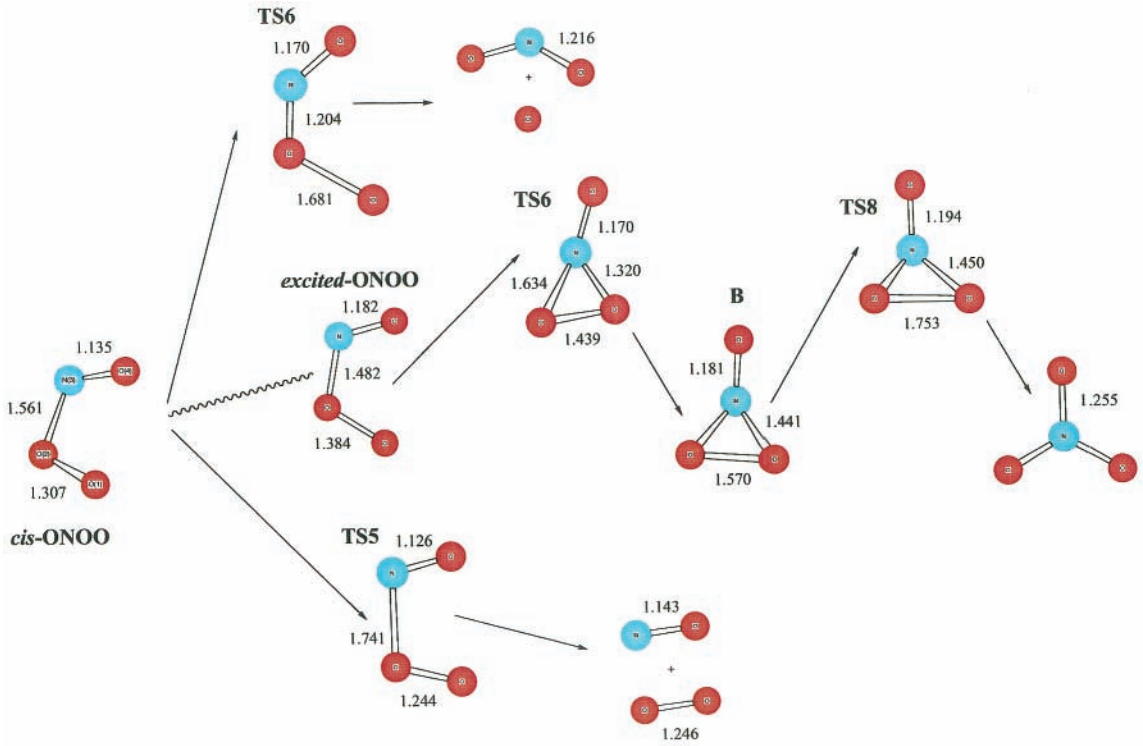

Figure 5. Final evolution of the peroxidic ONOO radical. Bond distances are given in angstroms.

used and the size of the basis set employed in the single-point QCISD(T) energy calculation is increased.

3.1.4. T_1 Diagnostic. The T_1 diagnostic gives a qualitative assessment of the significance of nondynamical correlation. Hence, it is used to ensure that all species involved in the mechanism of reaction 1 are well-treated with a single-reference-based wave function. We report in Table 4 the T_1 diagnostic values using the open-shell T_1 formalism of T. J. Lee et al.[49]

The larger the T_1 value, the less reliable the results of the single-reference coupled-cluster wave function are. For a closed-shell system, values over 0.02 are suspect, as happens with the ozone molecule as expected. However, Jayatilaka and Lee suggest that cut-off open-shell T_1 values may be larger. In fact, we found values of 0.045 accepted as reliable in the work of Rienstra-Kiracofe et al.,[50] so our highest values of 0.053 and 0.046 obtained for **TS1** and **TS2**, respectively, could be considered to be reliable enough.

Despite the multireference character of O_3, which shows a T_1 value of 0.027 at the CCSD(T)/6-311G(3d)//MP2/6-311G-(df) level, slightly greater than the recommended value of 0.020,

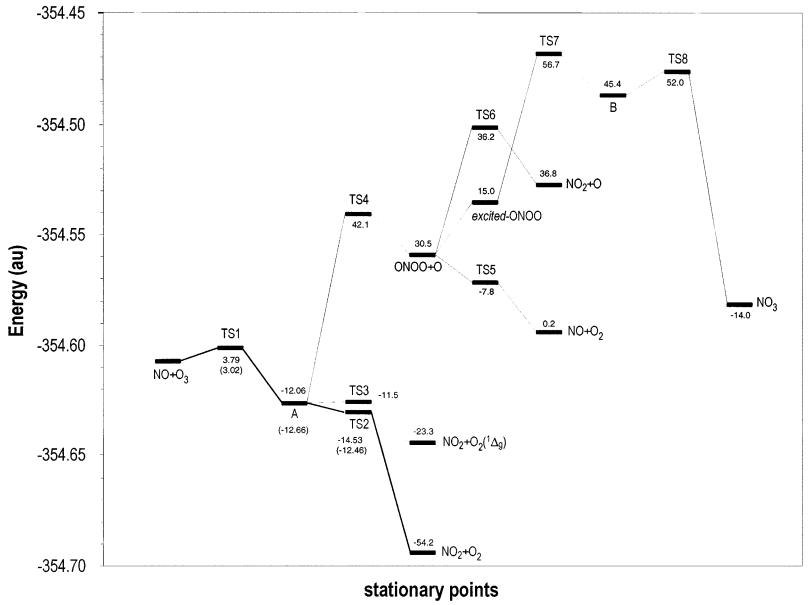

Figure 6. Potential QCISD(T)/6-311G(d)//UMP2(full)/6-31G(d) energy profile for the reaction between NO and O_3. Relative energies with respect to the reactants NO + O_3 are given in kcal/mol for all systems found until ONOO. After this system and the removal of an $O(^3P)$ atom, relative energies are given with respect to ONOO. Values in parentheses refer to the cis potential energy surface. ZPE and thermal corrections are included.

we will not appeal to complete active-space methodologies because of the difficulty in selecting a CAS consistent for all stationary points studied in this work.

3.2. NO + O_3 → NO_2 + $O_2(^1\Delta_g)$ Reaction. The mechanism for reaction 2 is depicted in Figure 4 along with the one for reaction 3 because the intermediate **A** is the starting point of both reactions. Reaction 2 takes place through the saddle point **TS3**, which is very similar to the **TS2** described for reaction 1. In fact, the largest differences are smaller than 0.045 Å. Thus, the only meaningful difference between **TS2** and **TS3** is the distribution of the atomic spin densities.

TS3 shows an imaginary frequency of 1136.0i cm^{-1} at the UMP2(full)/6-31G(d) level involving the asymmetric stretching of the N_2-O_3 and O_3-O_4 bonds in a similar way as for **TS2**. The estimation of ΔH_r^0 for this reaction is −23.39 kcal/mol. Then, reaction 2 is less exothermic than reaction 1.

The QCISD(T)/6-311G(d) barrier height corresponding to **TS3** is larger than the one corresponding to **TS2**. However, although there is no experimental evidence of the excited $O_2(^1\Delta_g)$ as a product, it cannot be neglected without further experimental research.

3.3. NO + O_3 → ONOO + $O(^3P)$ Reaction: Evolution of the ONOO Radical. In this last subsection, we will describe the mechanism of reactions 3−6. Figure 4 shows the mechanism of reaction 3. G2(MP2) and QCISD(T)/6-311G(d) reaction enthalpies and relative energies for reactions 2−6 are collected in Table 3S (Supporting Information) along with the vibrational frequencies calculated at the UMP2(full)/6-31G(d) level.

3.3.1. Reaction Mechanism and Energy Profile. The starting point of reaction 3 is the intermediate **A** in its trans conformation. This intermediate leads to ONOO through the saddle point **TS4**. Because reaction 3 is endothermic by 35.9 and 30.5 kcal/mol, respectively, at the G2(MP2) and QCISD(T)/6-311G(d)//UMP2/6-31G(d) levels of theory, **TS4** is located at the end of the reaction channel. Therefore, its geometry is very similar to that corresponding to the products ONOO + $O(^3P)$, which confirms the elongated bond distance of 1.991 Å between the terminal O atom and the forming ONOO radical in **TS4**.

The stationary point **TS4** has been characterized as a transition state with an imaginary frequency of 234.9i cm^{-1} that involves the elongation of the terminal oxygen−oxygen bond. The IRC carried out subsequently confirms the nature of **TS4**.

The ONOO radical has an unpaired electron on the terminal oxygen atom, as shown by the atomic spin-density value of 0.944 on it. This peroxidic radical can exist in two different conformations, the so-called *cis*-ONOO and *trans*-ONOO. Although we have focused only on the path leading toward the *trans*-ONOO through **TS4**, the pathway leading to the slightly more stable *cis*-ONOO also exists, and it would start in the *cis*-**A** intermediate. In any case, the pathway leading to the *cis*-ONOO does not contain different chemical information.

The peroxidic short-life ONOO radical is highly energetic, thus it will deactivate toward more stable products. As depicted in Figure 5, the ONOO radical can follow three different pathways giving NO + O_2, NO_2 + $O(^3P)$, or NO_3 as final stable products. Among them, the one leading to NO + O_2 is the most favored.

Reaction 4 involves the transition state *cis*-**TS5** with the cis conformation, as can be seen in Figure 5. The imaginary frequency of 1094.2i cm^{-1} associated with the reaction coordinate involves the stretching of the bond between the central N and O atoms. This transformation leads to the cleavage of that bond, as shown by the large value of the bond length of 1.741 Å.

TS5 exists, as the radical ONOO, in two different conformations: the so-called *cis*-**TS5** and *trans*-**TS5**. Furthermore, at the UMP2(full)/6-31G(d) level of theory, we have been able to optimize the homologous transition states leading to the $O_2(^1\Delta_g)$ excited state in both conformations.

The first step of reaction 6, as depicted in Figure 5, shows no saddle point. The reason is probably that the subsequent structure found via this route (excited ONOO) could be an electronic excited state of the *cis*-ONOO radical. When comparing the structure of the excited ONOO with the geometry of the ONOO ground state, we noticed that the bond lengths of both terminal bonds have increased from 1.307 to 1.384 Å and from 1.135 to 1.182 Å, whereas the central bond distance O_2-N_3 has decreased from 1.561 to 1.482 Å. This new structure shows enhanced radical character, as can be inferred from the

value of the total atomic spin density on the O_1 atom, which has increased from 0.933 to 1.072 in the excited ONOO molecule.

The excited ONOO is 15.0 kcal/mol above the ground state at the QCISD(T)/6-311G(d) level and leads to the intermediate **B** through the transition state **TS7**. The reaction coordinate involves a complex bending movement in which the N atom moves simultaneously toward O_1 and O_2. This stationary point has been characterized as a transition state with an imaginary frequency of 911.6i cm^{-1} and a barrier height of 41.6 kcal/mol at the QCISD(T)/6-311G(d) level, which means that it is a very slow path from a kinetic point of view.

At the next point in the reaction mechanism, the short-life intermediate **A** leads to the final stable product NO_3 through **TS8**. The reaction coordinate involves the enlargement of the distance between oxygen atoms O_1 and O_2. **TS8** has been characterized as a transition state with a single imaginary frequency of 792.2i cm^{-1}.

Reaction 5 involves the decomposition of the *cis*-ONOO radical into two more-stable fragments, NO_2 and $O(^3P)$, through the saddle point **TS6**. However, this seems very improbable because of the great barriers of 43.0 and 36.2 kcal/mol at the G2(MP2) and QCISD(T)/6-311G(d) levels, respectively, that must be overcome. This pathway, therefore, seems to be even slower than the one leading to NO_3.

Finally, to clearly summarize all the results obtained in this paper, we present in Figure 6 the profile of the mechanism found for the reaction between O_3 and NO at the QCISD(T)/6-311G-(d)//UMP2(full)/6-31G(d) level of theory.

4. Conclusions

A detailed study of reactions 1−6 has been presented by means of electronic structure calculations. The proposed reaction mechanism shows two different parts. One of them is highly improbable under atmospheric conditions of temperature and is related to reactions 2−6. The first step of the proposed mechanism for reaction 1, the other part, is the attack of the NO radical on one of the terminal oxygen atoms of the O_3 molecule following a π direction through the transition state **TS1**.

TS1 is the critical transition state determining the activation energy of reaction 1. The experimental activation energy recommended by IUPAC is 2.72 kcal/mol. Reaction 1 is thus an example of a fast reaction whose accurate energetics is quite difficult to study from both experimental and theoretical points of view. In fact, despite this recommended value, there is still great uncertainty because experimental reported measurements lie within the range 1.44−3.18 kcal/mol.

The QCISD(T)//UMP2 theoretical study predicts, corrected to 298.15 K, barrier heights within the range 4.94−1.63 kcal/mol, in agreement with experimental values.

Related to the reaction enthalpy, our best-estimated value is around −51 kcal/mol, slightly different from the experimentally measured value of −47.6 kcal/mol. However, it must be taken into account that the experimental value is an average of the values corresponding to the $NO_2(^2A_1)$ ground electronic state and to the $NO_2(^2B_2)$ excited state.

Finally, we point out that although the O_3 wave function has multiconfigurational character we have not appealed to multireference approaches. The reason lies in the difficulty of selecting a CAS that is consistent for all the stationary points calculated and because the single-reference CCSD(T) method is accurate enough[45] to describe the O_3 molecule reliably, despite the slightly large values of the T_1 diagnostic. However, multireference methods were definitively obviated because single- and multireference ab initio methods consistently predict the same results for the chemically equivalent system Cl + O_3[48] and because the rate-determining transition structure **TS1** obtained at the UMP2(full) level is equivalent to that optimized at the higher QCISD/6-31G(d) level.

Acknowledgment. J.P.-G. thanks the Conselleria d'Educació i Ciència for a personal grant. This work was supported by the Spanish DGES (Project PB97-1381) and CCEC (Projects INF99-02-134 and INF00-15).

Supporting Information Available: Geometrical parameters, vibrational frequencies, and total energies for transition states and reactants. This material is available free of charge via the Internet at http://pubs.acs.org.

References and Notes

(1) Atkinson, R.; Baulch, D. L.; Cox, R. A.; Rampson, R. F., Jr.; Kerr, J. A.; Troe, J. *J. Phys. Chem. Ref. Data* **1992**, *21*, 1125−1591.
(2) Suter, H. V.; Huber, J. R. *Chem. Phys. Lett.* **1989**, *155*, 203.
(3) Mebel, A. M.; Diar, E. W. G.; Lin, M. L.; Morokuma, K. *J. Phys. Chem.* **1996**, *100*, 7517.
(4) Hanway, D.; Fu-Ming, T. *Chem. Phys. Lett.* **1998**, *285*, 459−499.
(5) Blacet, F. E. *Ind. Eng. Chem.* **1952**, *44*, 1339.
(6) Leighton, P. A. *Photochemistry of Air Pollution*; Academic Press: New York, 1961.
(7) (a) Haagen-Smit, A. J. *Ind. Eng. Chem.* **1952**, *44*, 1342. (b) Haagen-Smit, A. J.; Fox, M. M. *J. Air Pollut. Control Assoc.* **1954**, *4*, 105. (c) Haagen-Smit, A. J., Fox, M. M. *SAE Trans.* **1955**, *63*, 575. (d) Haagen-Smit, A. J.; Fox, M. M. *Ind. Eng. Chem.* **1956**, *48*, 1484.
(8) Finlayson-Pitts, B. J.; Pitts, J. N., Jr. *Atmospheric Chemistry*; Wiley-Interscience: Chichester, U.K., 1986.
(9) Johnston, M. S. *Science (Washington, D.C.)* **1971**, *173*, 517.
(10) Graves, J. C.; Garvin, D. *J. Chem. Phys.* **1959**, *30*, 384.
(11) Taken from ref 23.
(12) Clyne, M. A. A.; Thrush, B. A.; Wayne, R. P. *Trans. Faraday Soc.* **1964**, *60*, 359.
(13) Clough, P. N.; Thrush, B. A. *Trans. Faraday Soc.* **1967**, *63*, 915.
(14) Stedman, D. H.; Niki, H. *J. Phys. Chem.* **1973**, *77*, 2604.
(15) Bemand, P. B.; Clyne, M. A. A.; Watson, R. T. *J. Chem. Soc., Faraday Trans.* **1974**, *70*, 564.
(16) Birks, J. W.; Shoemaker, B.; Leck, T. J.; Hinton, D. M. *J. Chem. Phys.* **1976**, *65*, 5181.
(17) Lippmann, H. H.; Jesser, B.; Schurath, U. *Int. J. Chem. Kinet.* **1980**, *12*, 547.
(18) Ray, G. W.; Watson, R. T. *J. Phys. Chem.* **1981**, *85*, 1673.
(19) Michael, J. V.; Allen, J. E., Jr.; Brobst, W. D. *J. Phys. Chem.* **1981**, *85*, 4109.
(20) Borders, R. A.; Birks, J. W. *J. Phys. Chem.* **1982**, *86*, 3295.
(21) Atkinson, R.; Baulch, D. L.; Cox, R. A.; Hampson, R. F., Jr.; Rossi, M. J.; Troe, J. *J. Phys. Chem. Ref. Data* **1997**, *26*, 1401−1402.
(22) Steinfeld, J. I.; Adler-Golden, S. M.; Gallagher, J. W. *J. Phys. Chem. Ref. Data* **1987**, *16*, 938−939.
(23) Dewar, M. J. S.; Zoebisch, E. G.; Healey, F.; Stewart, J. J. P. *J. Am. Chem. Soc.* **1985**, *107*, 3902.
(24) Vinson, L.; Dannenberg, J. J. *J. Am. Chem. Soc.* **1989**, *11*, 2777.
(25) Stewart, J. J. *MOPAC 93*. Technical report; Fujitsu Limited: Tokyo, Japan, 1993.
(26) Hurley, A. C. *Introduction to the Electron Theory of Small Molecules;* Academic Press: New York, 1976.
(27) (a) Becke, A. D. *J. Chem. Phys.* **1993**, *98*, 5648. (b) Becke, A. D. *J. Chem. Phys.* **1992**, *96*, 2155. (c) Becke, A. D. *J. Chem. Phys.* **1992**, *97*, 9173. (d) Lee, C.; Yang, W.;. Parr, R. G. *Phys. Rev. B* **1988**, *37*, 785.
(28) (a) Head-Gordon, M.; Pople, J. A.; Frisch, M. J. *Chem. Phys. Lett.* **1988**, *155*, 503. (b) Frisch, M. J.; Head-Gordon, M.; Pople, J. A. *Chem. Phys. Lett.* **1990**, *166*, 275. (c) Frisch, M. J.; Head-Gordon, M.; Pople, J. A. *Chem. Phys. Lett.* **1990**, *166*, 281. (d) Head-Gordon, M.; Head-Gordon, T. *Chem. Phys. Lett.* **1994**, *220*, 122. (e) Saebo, S.; Almlof, J. *Chem. Phys. Lett.* **1989**, *154*, 83.
(29) Hehre, W. J.; Radom, L.; Schleyer, P.; Pople, J. A. *Ab Initio Molecular Orbital Theory;* Wiley-Interscience: New York, 1986.
(30) Becke, A. D. *J. Chem. Phys.* **1993**, *98*, 5648.
(31) Perdew, J. P.; Wang, Y. *Phys. Rev. B* **1992**, *45*, 13244.
(32) (a) Hohenberg, P.; Khon, W. *Phys. Rev. B* **1964**, *136*, 864. (b) Khon, W.; Sham, L. J. *Phys. Rev. A* **1965**, *140*, 1133. (c) Slater, J. C. *Quantum Theory of Molecules and Solids*; International Series in Pure and Applied

Physics; McGraw-Hill: New York, 1974; Vol. 4. (d) Vosko, S. H.; Wilk, L.; Nusair, M. *Can. J. Phys.* **1980**, *58*, 1200.

(33) Schlegel, H. B. *J. Comput. Chem.* **1982**, *3*, 214.

(34) González, C.; Schlegel, H. B. *J. Chem. Phys.* **1989**, *90*, 2154.

(35) Baker, J. *J. Comput. Chem.* **1986**, *7*, 385.

(36) Scott, A. P.; Random, L. *J. Phys. Chem.* **1996**, *100*, 16502.

(37) Curtiss, L. A.; Raghavachari, K.; Pople, J. A. *J. Chem. Phys.* **1993**, *98*, 1293.

(38) Curtiss, L. A.; Raghavachari, K.; Trucks, G. W.; Pople, J. A. *J. Chem. Phys.* **1991**, *94*, 7221.

(39) (a) Pople, J. A.; Head-Gordon, M.; Raghavachari, K. *J. Chem. Phys.* **1987**, *87*, 5968. (b) Gauss, J.; Cremer, C. *Chem. Phys. Lett.* **1988**, *150*, 280. (c) Salter, E. A.; Trucks, G. W.; Bartlett, R. J. *J. Chem. Phys.* **1989**, *90*, 1752.

(40) (a) Pople, J. A.; Krishnan, R.; Schlegel, H. B.; Binkley, J. S. *Int. J. Quantum Chem.* **1978**, *14*, 545. (b) Cizek, J. *Adv. Chem. Phys.* **1969**, *14*, 35. (c) Purvis, G. D.; Bartlett, R. J. *J. Chem. Phys.* **1982**, *76*, 1910. (d) Scuseria, G. E.; Janssen, C. L.; Schaefer, H. F., III. *J. Chem. Phys.* **1988**, *89*, 7382. (e) Scuseria, G. E.; Schaefer, H. F., III. *J. Chem. Phys.* **1989**, *90*, 3700. (f) Bartlett, R. J.; Purvis, G. D. *Int. J. Quantum Chem.* **1978**, *14*, 516.

(41) Frisch, M. J.; Trucks, G. W.; Schlegel, H. B.; Gill, P. M. W.; Johnson, B. G.; Robb, M. A.; Cheeseman, J. R.; Keith, T.; Petersson, G. A.; Montgomery, J. A.; Raghavachari, K.; Al-Laham, M. A.; Zakrzewski, V. G.; Ortiz, J. V.; Foresman, J. B.; Cioslowski, J.; Stefanov, B. B.; Nanayakkara, A.; Challacombe, M.; Peng, C. Y.; Ayala, P. Y.; Chen, W.; Wong, M. W.; Andres, J. L.; Replogle, E. S.; Gomperts, R.; Martin, R. L.; Fox, D. J.; Binkley, J. S.; Defrees, D. J.; Baker, J.; Stewart, J. P.; Head-Gordon, M.; Gonzalez, C.; Pople, J. A. *Gaussian 94*, revision D.3; Gaussian, Inc.: Pittsburgh, PA, 1995.

(42) Herzberg, G. *Molecular Spectra and Molecular Structure;* Prentice-Hall Physics Series;Prentice-Hall: New York, 1966; Vol. 3.

(43) *Handbook of Chemistry and Physics*, 74th ed.; Lide, D. R., Ed.; CRC Press: Boca Raton, FL, 1993.

(44) Jensen, F. *Chem. Phys. Lett.* **1990**, *169*, 519.

(45) García-Cuesta, I.; Sánchez-Marín, J.; Sánchez de Merás, A.; Ben Amor, N. *J. Chem. Phys.* **1997**, *107*, 6306.

(46) Dupuis, M.; Fitzgerald, G.; Hammond, B.; Lester, W. A.; Schaefer, H. F. *J. Chem. Phys.* **1986**, *84*, 2691.

(47) Hammond, G. S. *J. Am. Chem. Soc.* **1955**, *77*, 334.

(48) Hwang, D.; Mebel, A. M. *J. Chem. Phys.* **1998**, *109*, 10847.

(49) Lee, T. J.; Taylor, P. R. *Int. J. Quantum Chem., Symp.* **1989**, *23*, 199.

(50) Rienstra-Kiracofe, J. C.; Allen, W. D.; Schaefer, H. F., III. *J. Phys. Chem. A* **2000**, *104*, 9823.